Seasonal Sensitivity of the Eddy-Driven Jet to Tropospheric Heating in an Idealized AGCM

MARIE C. MCGRAW AND ELIZABETH A. BARNES

Department of Atmospheric Science, Colorado State University, Fort Collins, Colorado

(Manuscript received 14 October 2015, in final form 23 February 2016)

ABSTRACT

A dry dynamical core is used to investigate the seasonal sensitivity of the circulation to two idealized thermal forcings: a tropical upper-tropospheric heating and a polar lower-tropospheric heating. The thermal forcings are held constant, and the response of the circulation in each month of the year is explored. First, the circulation responses to tropical warming and polar warming are studied separately, and then the response to the simultaneously applied forcings is analyzed. Finally, the seasonality of the internal variability of the circulation is explored as a possible mechanism to explain the seasonality of the responses. The primary results of these experiments are as follows: 1) There is a seasonal sensitivity in the circulation response to both the tropical and polar forcings. 2) The jet position response to each forcing is greatest in the transition seasons, and the jet speed response exhibits a seasonal sensitivity to both forcings, although the seasonal sensitivities are not the same. 3) The circulation response is nonlinear in the transition seasons, but approximately linear in the winter months. 4) The internal variability of the unforced circulation exhibits a seasonal sensitivity that may partly explain the seasonal sensitivity of the forced response. The seasonality of the internal variability of daily MERRA reanalysis data is compared to that of the model, demonstrating that the broad conclusions drawn from this idealized modeling study may be useful for understanding the jet response to anthropogenic forcing.

1. Introduction

One of the most robust signs of climate change is the poleward shift of the midlatitude eddy-driven jets and storm tracks (Collins et al. 2013). The IPCC Fifth Assessment Report (AR5) states that poleward shifts of the midlatitude eddy-driven jets are likely by the end of the twenty-first century under the strongest forcing scenario, Representation Concentration Pathway 8.5 (RCP8.5) (Collins et al. 2013), and Barnes and Polvani (2013) find that all 22 phase 5 of the Coupled Model Intercomparison Project (CMIP5) models they examined project a poleward shift of the Southern Hemisphere eddy-driven jet by the end of the twenty-first century (see their Fig. 1a). The robustness of the Southern Hemisphere jet response in the CMIP5 and CMIP3 models has been well documented (e.g., Barnes and Polvani 2013; Yin 2005). However, there is uncertainty and low confidence in the response of the Northern Hemisphere eddy-driven jet to anthropogenic climate change. This uncertainty is due, in part, to the competing effects of tropical upper-tropospheric warming and polar near-surface warming on the midlatitude circulation (e.g., Held 1993; Holland and Bitz 2003; Harvey et al. 2014; Deser et al. 2015). Thus, a critical component of reducing the uncertainty in the future response of the Northern Hemisphere jet streams is understanding the circulation response to these low- and high-latitude tropospheric warmings.

Although the earth system response to anthropogenic forcing is and will comprise many complex interactions between the atmosphere, ocean, and land surface, the dynamics describing the response of the eddy-driven jet are thought to be likely governed, at least in part, by dry dynamics. Idealized dry models do, in fact, simulate the same sign of the large-scale response to various climate-change-like warmings as are found in the state-of-the-art climate models (e.g., Tandon et al. 2011; Butler et al. 2010). Therefore, idealized models can act as a test bed for exploring the responses of the eddy-driven jet to climate-change-like forcings, and are an efficient and effective way for developing and testing hypotheses that

Corresponding author address: Marie C. McGraw, Department of Atmospheric Science, Colorado State University, 1371 Campus Delivery, Fort Collins, CO 80523.
E-mail: mmcgraw@atmos.colostate.edu

DOI: 10.1175/JCLI-D-15-0723.1

describe the dynamics of these responses. For example, Polvani and Kushner (2002) and Kushner and Polvani (2004) demonstrate that the eddy-driven jet shifts poleward in response to polar stratospheric cooling in a dry dynamical core; similar to the observed positive trend in the southern annular mode noted by Thompson and Solomon (2002) that is attributed to polar stratospheric cooling due to ozone depletion. Wang et al. (2012) and Butler et al. (2010) note a poleward shift of the eddy-driven jet in response to tropical upper-tropospheric heating in a dry dynamical core, consistent with the responses in the current state-of-the-art general circulation models (GCMs) (e.g., Barnes and Polvani 2013). Butler et al. (2010) describe the circulation response to three thermal forcings attributed to anthropogenic warming in a dry dynamical core: a poleward shift of the storm tracks in response to polar stratospheric cooling and tropical upper-tropospheric warming, and an equatorward shift of the storm tracks in response to polar surface warming. They suggest that the mechanisms behind these shifts of the storm tracks are driven by dry dynamics, demonstrating that these simple, idealized models can in fact be used to investigate many of the processes driving future changes in the midlatitude jet streams.

The sign of the eddy-driven jet response to tropical upper-tropospheric warming and to polar lower-tropospheric warming is considered largely robust (e.g., Held 1993; Butler et al. 2010); however, the magnitude of the response is likely sensitive to several factors. For example, it has been well documented (e.g., Kidston and Gerber 2010; Son et al. 2010) that the climatological position of the jet stream is important in determining the magnitude of the jet response; that is, jets that are climatologically more equatorward tend to shift more than jets that are climatologically located farther poleward. This sensitivity is likely tied to the fact that the variability of the midlatitude eddy-driven jet is also sensitive to the climatological jet position, with more equatorward jets exhibiting more persistence and less variability (e.g., Barnes et al. 2010; Kidston and Gerber 2010), and that this variability is tightly coupled to the jet response through the fluctuation–dissipation theorem (e.g., Gerber et al. 2008; Shepherd 2014; Ring and Plumb 2007, 2008). Given that the state-of-the-art GCMs are known to have equatorward biases in their placements of the jets, it is possible that they also overestimate the shifts of the eddy-driven jets at the end of the twenty-first century.

The eddy-driven jet response to anthropogenic forcing may also be sensitive to the state of the subtropical circulation. The subtropical jet strength can impact the position of the eddy-driven jet (and thus, potentially, the eddy-driven jet response) by controlling the location of the baroclinic region (e.g., Son and Lee 2005). Garfinkel et al. (2013) demonstrated that the magnitude of the jet shift driven by changes in the stratospheric polar vortex strength decreased as the climatological jet position was located closer to the subtropics. Since the leading mode of eddy-driven jet variability has been shown to depend on the position and strength of the subtropical jet (e.g., Eichelberger and Hartmann 2007; Barnes and Hartmann 2011), and the jet response to external forcing is coupled to its internal variability, it is likely that the state of the subtropical circulation may play a role in determining the zonally symmetric jet response to anthropogenic climate change.

It is well known that the strength and position of the eddy-driven jet varies with season in observations [e.g., Fig. 1a of Hannachi et al. (2013)], as does the variability (e.g., Eichelberger and Hartmann 2007; Simpson et al. 2013). Additionally, the strength and meridional extent of the subtropical jet also exhibits a seasonal cycle (e.g., Davis and Birner 2013). Therefore, it is possible that the seasonality of the jet dynamics throughout the year could alone drive seasonality in the jet response to climate change. However, previous atmosphere-only GCM (AGCM) studies on the jet response to thermal forcings have tended to focus on the response in a single season—Polvani and Kushner (2002), Kushner and Polvani (2004), and Wang et al. (2012) focus solely on winter, while Butler et al. (2010) primarily focus on the equinoctal state (although they do briefly explore the wintertime response). Kushner and Polvani (2006) explore the sensitivity of the tropospheric response to a stratospheric seasonal cycle, but do not apply a seasonal cycle to the troposphere. Deser et al. (2010) explore the seasonality of the atmospheric response to projected sea ice loss using an AGCM coupled to a land surface model, but they hold greenhouse gas concentrations constant, and force the model with seasonal variations in sea ice and sea surface temperature (SST). Thus, although Barnes and Polvani (2013) note that the Northern and Southern Hemisphere jet shifts under RCP8.5 vary seasonally by over 1° latitude across seasons, it is unclear how much of this seasonality is due to the seasonality of the jet dynamics, and how much is due to seasonality of the forcing.

In this work, the seasonality of the circulation response to two idealized thermal forcings is investigated using a dry dynamical core. The first of these is a tropical upper-tropospheric warming, intended to simulate the effects of increased latent heating in the tropical upper troposphere due to anthropogenic forcing. The second of these heatings is a polar lower-tropospheric warming, meant to simulate Arctic amplification; that is, the

preferential warming of the Arctic when compared to the global mean surface temperature increase due to climate change (e.g., Holland and Bitz 2003). This work focuses on these two heatings, as the uncertainty in the projections of the Northern Hemisphere circulation response is in large part due to the opposing signs of the responses to tropical upper-tropospheric heating and Arctic amplification (e.g., Harvey et al. 2014). The experiments presented here are set up such that the heatings are held constant throughout the simulations, while the tropospheric circulation is given a seasonal cycle by varying the tropospheric relaxation temperature profile. Although these thermal forcings do in fact vary seasonally in reality, particularly Arctic amplification (e.g., Deser et al. 2010), this framework allows for the separation of seasonal variations in the heating from the seasonal sensitivity of the circulation response to the heating.

The simulations have been run with 20 vertical levels and tropospheric dynamics only. While stratospheric dynamics and stratosphere–troposphere coupling certainly affect tropospheric jet dynamics and variability (e.g., Thompson and Birner 2012; Butler et al. 2011; Polvani and Kushner 2002), stratospheric dynamics are not thought to be the singular driver of the tropospheric jet response to anthropogenic forcing. Simpson et al. (2012) and Garfinkel et al. (2013) suggest that the tropospheric jet response to anthropogenic forcing is primarily governed by tropospheric dynamics (e.g., the strength of tropospheric eddy–mean flow feedbacks, changes in eddy momentum fluxes, and the strength of jet persistence). A more complete discussion of this topic can be found in section 5 of Garfinkel et al. (2013). Therefore, it is not unreasonable to focus primarily on the tropospheric response and circulation. Furthermore, several previous studies (e.g., Kushner and Polvani 2006; Sheshadri et al. 2015) have already explored the impacts of the stratospheric seasonal cycle and seasonal variability of the polar vortex strength on the tropospheric circulation, and so, the experiments described here have been designed to evaluate the role of the tropospheric circulation's seasonal sensitivity in isolation.

The model and experimental framework are discussed in section 2. Section 3 describes the circulation response to the individual thermal forcings, the circulation response to the combination of both forcings, and the sensitivity of the results to the climatological position of the eddy-driven jet. Section 4 explores a possible explanation for the seasonality of the circulation response, and briefly compares the model results to observations. Section 5 presents the conclusions of this work.

2. Experimental setup

a. Model

All experiments performed in this study use the Geophysical Fluid Dynamics Laboratory (GFDL) spectral dry dynamical core. The model is run at T42 resolution with 20 evenly spaced sigma levels, and a time step of 1200 s. Zonal wind and temperature data in both daily and monthly (defined as 30-day means) temporal resolutions are analyzed here. Except where indicated, results are calculated using monthly data. The model configuration is zonally and hemispherically symmetric; thus, only results for the Northern Hemisphere will be shown. While topography is important in the full Northern Hemisphere circulation response to tropospheric heating (e.g., Shaw and Voigt 2015), the focus of this study is on the zonally symmetric response to tropospheric heating. Therefore, topography has been excluded from these experiments. Model parameters are identical to those used in Held and Suarez (1994, hereafter HS94), except where noted.

To simulate radiative processes, HS94 define the model's relaxation temperature profile as

$$T_{\rm eq}^{\rm trop}(p,\phi) = \max\left[200\,{\rm K}, (T_0 - \delta T_{\rm HS94})\left(\frac{p}{p_0}\right)^{\kappa}\right], \qquad (1)$$

with $T_0 = 315\,{\rm K}$, and $p_0 = 1000\,{\rm hPa}$. The term max is a maximum function that does not allow the atmospheric temperature to drop below 200 K. This is especially important in the upper levels of the model—since this model configuration does not have realistic stratospheric dynamics, the max function largely determines the temperature above the tropopause. The importance of the 200-K minimum temperature is discussed in more detail in the appendix. As in Polvani and Kushner (2002), $\delta T_{\rm HS94}$ is modified from HS94 in order to simulate a seasonal cycle, namely, by introducing a hemispheric asymmetry in the radiative equilibrium temperature profile:

$$\delta T_{\rm HS94} = (\Delta T)_y \sin\phi^2 + \varepsilon\chi\sin\phi + (\Delta T)_z \log\left(\frac{p}{p_0}\right)\cos\phi^2, \qquad (2)$$

where ϕ is the latitude in degrees, $(\Delta T)_y = 60\,{\rm K}$, $(\Delta T)_z = 10\,{\rm K}$, and ε determines the magnitude of the hemispheric asymmetry. The amplitude of ε is set to 20 K, following Chen and Plumb (2014). Increasing the amplitude of ε from the often-used value of 10 K (e.g., Polvani and Kushner 2002) has the dual effect of enhancing the hemispheric asymmetry and improving the basic state of the model, by producing a stronger

TABLE 1. Values of χ from Eq. (2) for every month.

Month	χ	Month	χ
Jan	+0.9659	Jul	−0.9659
Feb	+0.7071	Aug	−0.7071
Mar	+0.2588	Sep	−0.2588
Apr	−0.2588	Oct	+0.2588
May	−0.7071	Nov	+0.7071
Jun	−0.9659	Dec	+0.9659

subtropical jet and a more poleward eddy-driven jet. Here χ is a multiplier that modifies the value of ε based on the season. At the Northern Hemisphere winter solstice, when the asymmetry between the two hemispheres is greatest, χ is set to 1 (and $\chi = -1$ for Northern Hemisphere summer). On the equinoxes, when the asymmetry between the two hemispheres is zero, χ is set to 0. Many previous studies have run this model under solstice conditions, so χ is assumed to be 1 and is not explicitly mentioned in those studies. Six different values of χ were chosen to simulate six months of the year; the other six months were assumed to be symmetric. So, although only six separate values of χ were simulated, the results are presented in a 12-month format to visualize the full seasonal cycle. The values of χ used for each month are listed in Table 1.

b. Control runs

The first family of experiments uses the model default configuration, described in (1) and (2). For each experiment, each month is run separately under perpetual conditions (i.e., perpetual January, perpetual February, etc.). For each of the six values of χ seen in Table 1, two separate 50-yr simulations are run and then averaged together. Thus, each experiment actually comprises 12 separate simulations, 2 for each value of χ. First, two 50-yr control experiments (referred to as CTRL) with no heating are run for each value of χ, with the first 2 years discarded for spinup. The heating experiments, described in detail in the next section, branch off of these control runs, and follow the same structure of two 50-yr runs for each value of χ that are subsequently averaged together.

In all experiments, the primary variables of interest are the eddy-driven jet position and strength. As is common practice, the jet position is defined by identifying the maximum of the zonal mean zonal wind on the 775-hPa surface, and then fitting a second-order polynomial through the maximum. The location and magnitude of the maximum of the polynomial are the jet position and strength, respectively. This quantity is often calculated by averaging over several pressure levels (e.g., Woollings et al. 2010); in these simulations, the vertically averaged results are almost identical to the results obtained using only 775 hPa. Thus, only a single pressure level is used for simplicity.

The mean jet position and strength for each month's control run (CTRL experiment) are shown in Fig. 1. As seen in Fig. 1a, the seasonal cycle of the jet position is more poleward in summer than in winter, although the jet is most equatorward in the transition seasons (February–November and March–October). The jet is located between 40° and 50°N. These latitudes are comparable to the observed mean monthly latitudes of the North Atlantic jet [see Fig. 1a in Hannachi et al. (2013)]. The mean jet strength, seen in Fig. 1b, is strongest in the winter, when temperature gradients are strongest and baroclinicity is greatest, and weakest in the summer, when temperature gradients and baroclinicity are weakest. The jet strengths vary from about 18 to about 10 m s^{-1}. Again, these values are comparable to the observed North Atlantic jet strength [see Fig. 1b in Hannachi et al. (2013)].

c. Heating experiments

At the end of each month's control simulation, two thermal forcing experiments are run. The first experiment, TROP, simulates the tropical upper-tropospheric warming due to increased latent heating [a signature of greenhouse gas warming, see Fig. 12 in Collins et al. (2013)]. The second experiment, POLAR, simulates the polar lower-tropospheric warming associated with Arctic amplification (e.g., Holland and Bitz 2003). The heating experiments branch off of the end of the control runs and run for another 50 years, with the first 2 years (the transient adjustment period) discarded. So, the January tropical heating experiment branches off of the end of the January control experiment, and so on. The thermal forcings are turned on at the beginning of the runs, and remain constant throughout the simulations. Most importantly, the strength and location of the heating is identical in every month.

Following Butler et al. (2010), the zonally symmetric forcing, F, is defined as

$$F = q_0 \exp\left\{-\left[\frac{(x-x_0)^2}{2\sigma_x^2} + \frac{(z-z_0)^2}{2\sigma_z^2}\right]\right\}, \qquad (3)$$

where q_0 is the amplitude of heating, x is the latitude (in radians), and z is the sigma level. Thus, the heating is Gaussian in x and z. The heating amplitude, q_0, is different for TROP (0.3 K day^{-1}) and POLAR (1.0 K day^{-1}), and does not vary unless otherwise noted. The POLAR heating amplitude is larger than the TROP heating amplitude because the Arctic is projected to warm more relative to other parts of the globe [see Fig. 10 in Collins et al. (2013)]. The additional parameters in (3) are given in Table 2.

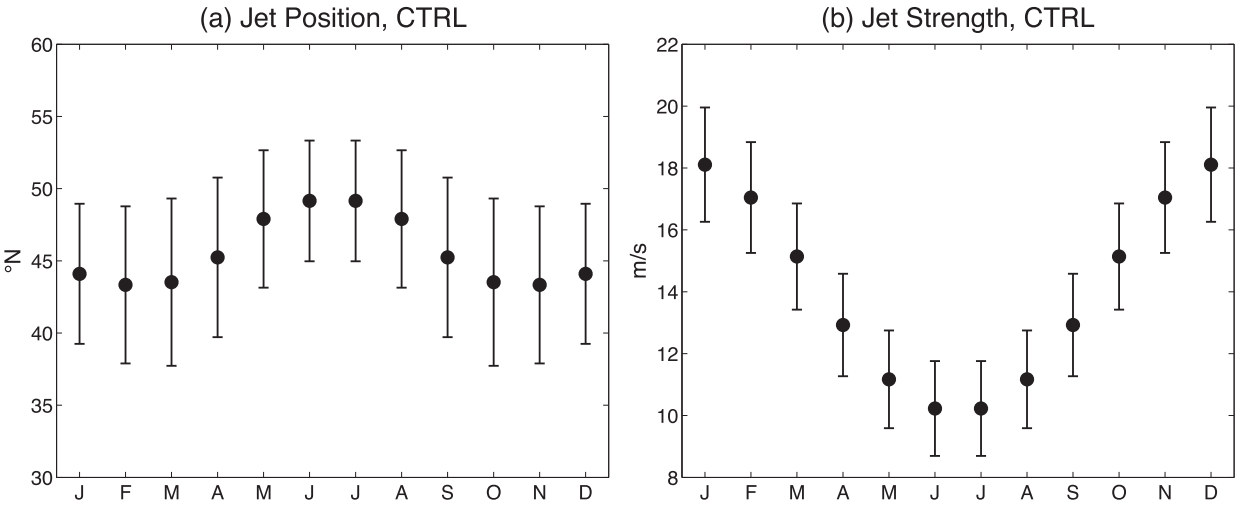

FIG. 1. Mean (a) jet position and (b) strength for model control runs. Error bars indicate the 5th and 95th percentile range to show the internal variability of the jet.

The zonal mean heating profiles for TROP and POLAR are plotted in Figs. 2a and 2b, respectively. The heating in the TROP experiment (Fig. 2a) represents the signature of greenhouse gas warming—a rise in temperatures in the tropical upper troposphere due to increased water vapor. The POLAR experiment simulates Arctic amplification—the lower-level polar warming attributed, in part, to an ice-albedo feedback (e.g., Screen and Simmonds 2010). Several configurations of Arctic amplification experiments were run, with variations of the vertical position (centered at 750 and 1000 hPa), vertical thickness (125 and 250 hPa), and amplitude of heating (0.5 and 1.0 K day^{-1}). While the magnitude of the jet response does change in response to these different heating profiles, the seasonal sensitivity of the jet response is similar across all experiments. Thus, these results are robust across a wide range of polar heating profiles.

d. Adjustment of mean state

The second set of experiments tests the seasonal sensitivity of the jet response to the climatological position of the jet. The mean jet position is varied by further modifying the background equilibrium temperature profile in a manner consistent with previous studies (e.g., Simpson et al. 2010; Garfinkel et al. 2013). These modifications to the background equilibrium temperature profile change the mean meridional position of the jet without having a large impact on the jet speed or eddy heat and momentum fluxes. To do this, the δT_{HS94} term [in (2)] is modified further, following Garfinkel et al. (2013):

$$pt\delta T_{\mathrm{new}} = \delta T_{\mathrm{HS94}} + A\cos[2(\phi - 45)]P(\phi), \tag{4a}$$

$$T_{\mathrm{eq}}^{\mathrm{trop}}(p,\phi) = \max\left[200\,\mathrm{K}, (T_0 - \delta T_{\mathrm{new}})\left(\frac{p}{p_0}\right)^{\kappa}\right], \tag{4b}$$

where $P(\phi) = \sin[4(\phi - 45)]$, and ϕ is latitude in degrees. Note that the full equation used by Garfinkel et al. (2013) includes a third term that depends on a parameter, B. However, as B is set to zero throughout this study, that term has been dropped from (4a) for simplification. Increasing A shifts the jet poleward, and decreasing A shifts the jet equatorward. While the shape of the equilibrium temperature profile changes slightly [see Fig. 2 in Garfinkel et al. (2013)], the equator-to-pole temperature difference does not change.

Four different values of A were tested in this set of experiments: $A = \pm 5.0$, referred to as A+5 and A−5, respectively; and $A = \pm 2.0$, referred to as A+2 and A−2, respectively. Here A+5 is similar to the GCM49 experiment in Barnes and Thompson (2014), and A+2 and A−2 are similar to the TR4 and TR2 experiments in Simpson et al. (2010). Each of these four experiments is also initiated with two separate 50-yr control runs for each value of χ, and averaged together. Similar to the first set of experiments, the TROP and POLAR heat

TABLE 2. Parameters for thermal forcings for TROP and POLAR. Here q_0 is heating amplitude; x_0 and z_0 are the horizontal and vertical centers of heating, respectively; and σ_x and σ_z are the horizontal and vertical half-widths of heating, respectively.

Expt name	q_0 (K day^{-1})	$x_0 \pm \sigma_x$ (°)	$z_0 \pm \sigma_z$ (hPa)
TROP	0.3	0 ± 27	300 ± 125
POLAR	1.0	90 − 16	1000 + 250

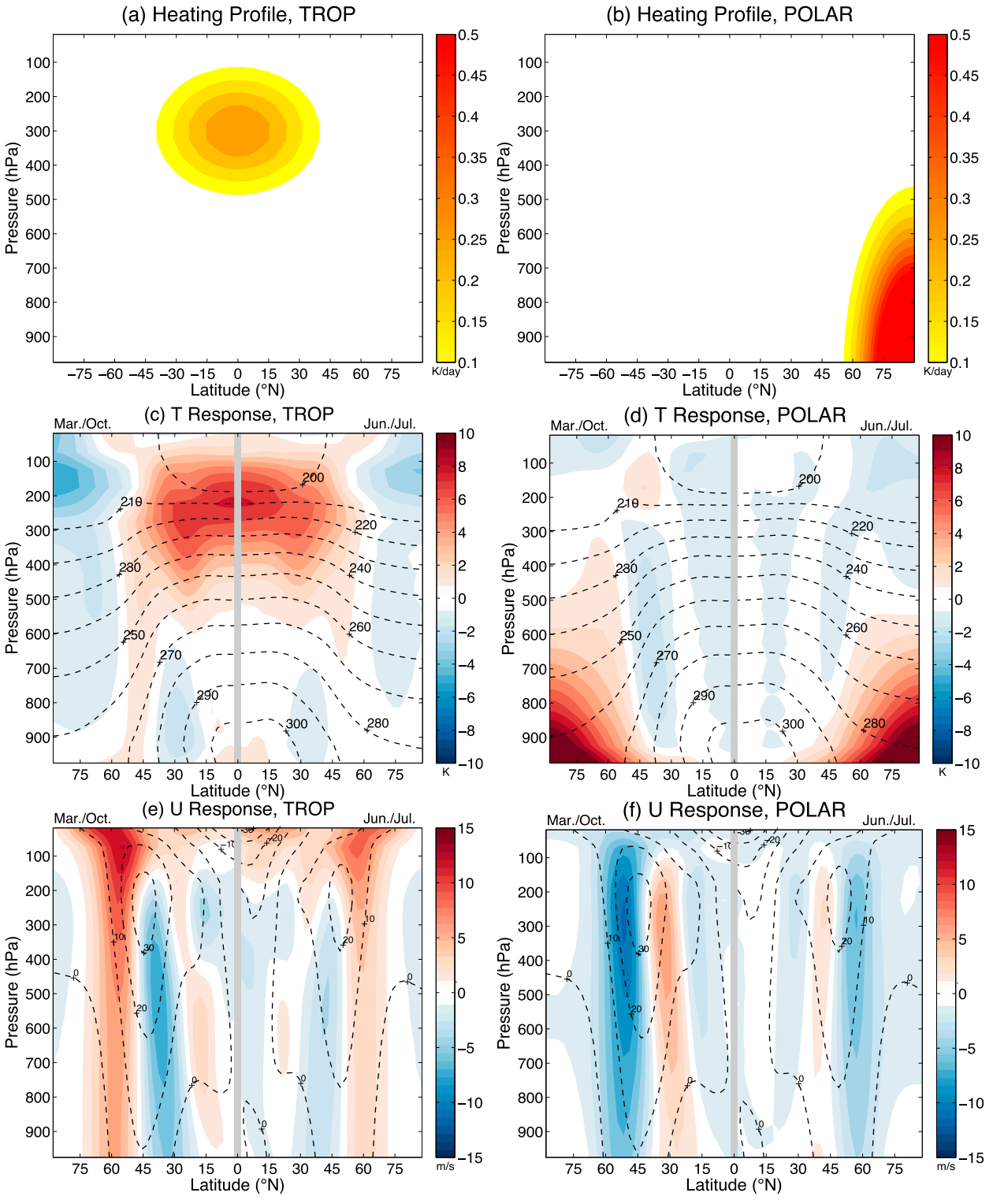

FIG. 2. Zonal mean (a),(b) heating profiles; (c),(d) temperature responses; and (e),(f) zonal wind responses for the Northern Hemisphere. Dashed lines indicate the temperatures and winds from CTRL, while colors indicate the anomalies for (c),(e) TROP and (d),(f) POLAR. For (c),(d),(e),(f), the March–October response is shown on the left, and the June–July response is shown on the right.

forcings described in Table 2 are applied at the end of each control run, and run for an additional 50 years. The results of these mean state experiments are then compared to the first set of experiments to determine the sensitivity of the circulation response to the mean position of the jet.

e. *Reanalysis data*

In the final part of this study, the daily Modern-Era Retrospective Analysis for Research and Applications (MERRA) reanalysis data (Rienecker et al. 2011) is used to compare the idealized modeling results with observations. The MERRA data have a horizontal spatial resolution of 1.25° × 1.25°. For simplicity, this analysis is restricted to the North Atlantic region, which is defined as extending from 15°–75°N to 0°–70°W. The daily zonal mean zonal wind (U) from January 1979 to December 2010 is vertically averaged over four levels—925, 850, 775, and 700 hPa—and used to calculate the eddy-driven jet position and strength using the method described in section 2b. As in previous studies (e.g., Woollings et al. 2010), a 10-day Lanczos filter with 61 weights is applied to the daily data before the jet position and strength are calculated, removing the features associated with higher-frequency synoptic variability and preserving only the low-frequency variability of the eddy-driven jet. This 10-day Lanczos filter is also applied to the vertically averaged zonal wind fields used to calculate the e-folding time of the first principal component time series of the zonal-mean zonal wind (see section 4 for more information about this calculation).

3. Results

a. *Model response to a single thermal forcing*

The Northern Hemisphere zonal mean temperature and zonal wind responses for the TROP and POLAR experiments are shown in Fig. 2. For Figs. 2c–f, the June–July response is shown on the right, and the March–October response is shown on the left. March–October and June–July were chosen as they are the months of greatest contrast. For both the TROP (Fig. 2c) and POLAR (Fig. 2d) experiments, the largest temperature response is seen where the heating is applied, and the response outside this region is smaller and/or negative.

The zonal wind responses for TROP (Fig. 2e) and POLAR (Fig. 2f) exhibit a seasonality in their responses. For example, the zonal wind response for TROP (Fig. 2e) shows a poleward shift in the eddy-driven jet (indicated by the positive zonal wind anomalies centered around 60°N) in both June–July (right) and March–October (left). These positive zonal wind anomalies extend vertically throughout the troposphere. The zonal wind response in POLAR (Fig. 2f) shows an equatorward shift of the jet in both June–July (right) and March–October (left), indicated by the negative anomalies centered around 55°N and the positive anomalies centered around 30°N.

The zonal wind responses to the two imposed heatings—a poleward shift in response to TROP, and an equatorward shift in response to POLAR—have been previously observed in many studies (e.g., Ring and Plumb 2008; Butler et al. 2010). The sign of this response is often attributed to meridional changes in the temperature field. For example, imposing a heating in the tropical upper troposphere would be expected to warm the tropical atmosphere at upper levels, while the polar atmosphere at the same vertical heights would not be expected to warm. This would increase the horizontal equator-to-pole temperature difference, which would increase the upper-level winds based on thermal wind balance. Chen and Held (2007) hypothesize that this increase in the upper-level winds would increase the Rossby wave phase speed, which would shift the eddy momentum flux convergence (and thus, it follows, the eddy-driven jet) poleward. The equatorward shift of the jet in response to a polar low-level warming is suggested to be a response to changes in lower-level baroclinicity due in part to changes in the lower-level equator-to-pole temperature gradient caused by the polar warming (e.g., Deser et al. 2010). Others have suggested a role for stratospheric pathways in determining the tropospheric circulation response to high-latitude warming. One such example is that zonally asymmetric high-latitude warming can modify the stationary wave patterns, which then influence the jet stream through stratosphere–troposphere coupling (e.g., Cohen et al. 2007). As the focus of this work is on tropospheric dynamics, these hypotheses will not be explored here but are explored in Wu and Smith (2016) in a similar idealized framework.

For all following analysis, the midlatitude circulation is quantified as the response of the midlatitude jet position and strength using the metrics described previously. The monthly mean jet positions for TROP and POLAR are compared to those of CTRL in Fig. 3a. Throughout this study, the responses to the tropical heating are shown in red, while the responses to the polar heating are shown in blue. The seasonal cycle exhibited by the jet in the CTRL experiment is preserved in the heating experiments—in all experiments, the jet is farther poleward in summer than in winter. In the TROP experiment, the jet position seasonal cycle is flatter than that of CTRL; that is, the difference between the most

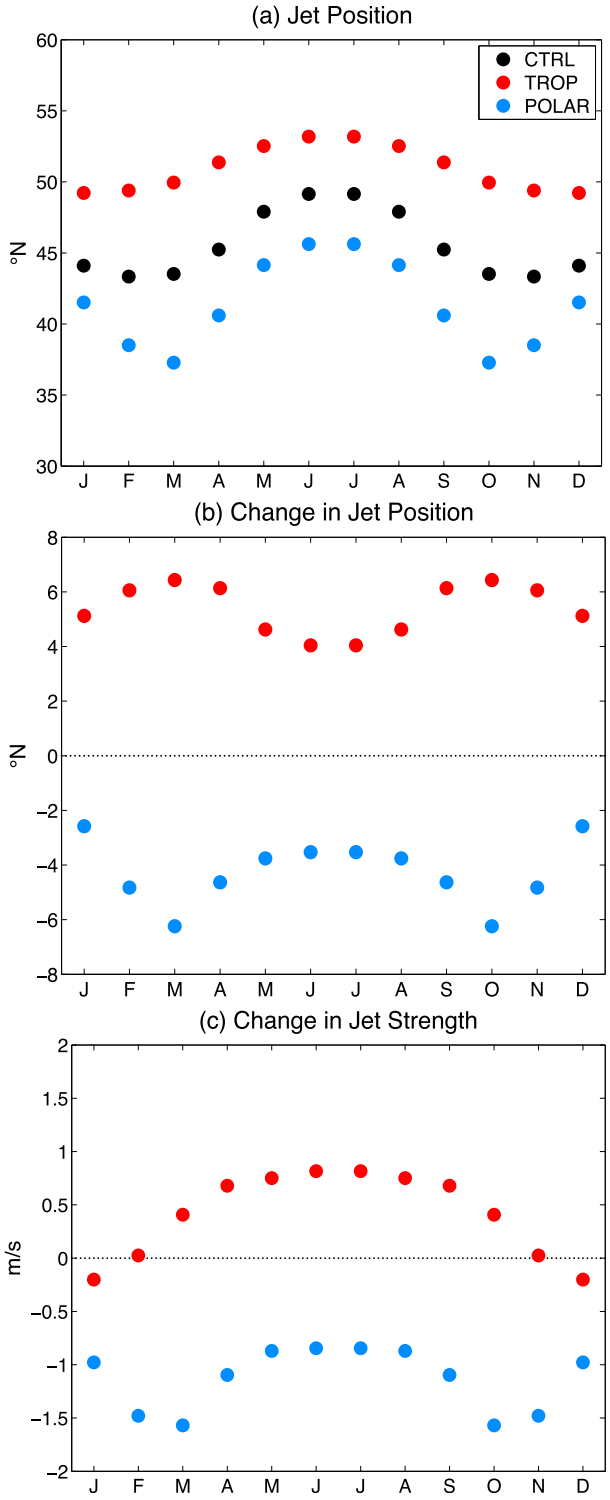

FIG. 3. (a) Jet position, (b) change in jet position, and (c) change in jet strength for TROP and POLAR heating experiments.

poleward and most equatorward months is smaller in the TROP experiment than it is in the CTRL experiment. In contrast, the seasonal cycle of the jet position is enhanced in the POLAR experiment—the difference between the most poleward month and the most equatorward month is greater for the POLAR experiment when compared to the CTRL experiment.

Figure 3b compares the jet position response in the TROP and POLAR experiments. The jet position response is defined as the change in jet position for the heating experiments as compared to the CTRL experiment. Consistent with previous modeling studies (e.g., Butler et al. 2010), the jet shifts poleward in every month in response to a tropical upper-tropospheric heating (the TROP experiment), and equatorward every month in response to a polar lower-tropospheric heating (the POLAR experiment). However, although the sign of the response is the same, Fig. 3b clearly indicates that the amplitude of the response to both TROP and POLAR varies across months. Since an identical thermal forcing is applied in each month, these differences in the amplitude of the response show that there is a seasonal sensitivity in the circulation response to tropospheric heating. The amplitude of the circulation response is largest in the transition seasons for both of the heating experiments, with smaller responses occurring in the summer and the winter months. The differences between the months with the largest response (March–October for both TROP and POLAR) and the month with the smallest response (June–July for TROP, January–December for POLAR) exceeds 3° latitude. Many studies evaluate the circulation response to simulated climate change either in the annual mean or in the winter (e.g., Ring and Plumb 2008; Polvani and Kushner 2002). However, Fig. 3b demonstrates that this would lead to an underestimation of the maximum amplitude of the circulation response in this model.

Similar to Fig. 3b, Fig. 3c displays the response of the jet strength. The seasonal cycles of jet strength for TROP and POLAR are similar to that of CTRL (not shown; the seasonal cycle of jet strength for CTRL can be seen in Fig. 1b), with the jet strongest in winter and weakest in summer. However, the jet position and strength responses do not exhibit the same seasonal sensitivity to the TROP heating. The jet strength changes most in the summer, strengthening by up to $1\,\mathrm{m\,s^{-1}}$. In contrast, the response in the winter months is weak, and even negative (indicating a weakening of the jet) in January–December. The jet strength response to POLAR, however, does have a similar seasonal sensitivity to that of jet position; namely, the jet strength response is negative in all months, indicating a weakening of the jet, and is largest in March–October.

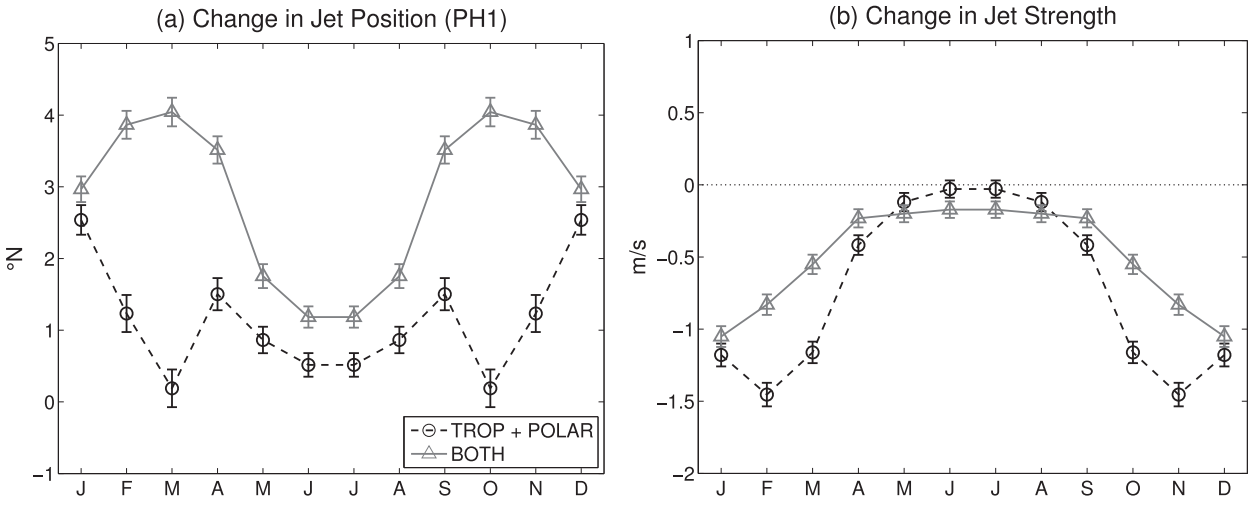

FIG. 4. Change in (a) jet position and (b) jet strength for BOTH and TROP + POLAR heating experiments. Here, the error bars indicate the confidence bounds calculated using a standard comparison of means between BOTH and TROP + POLAR at 95% confidence.

The contrasts between the jet position and strength responses in the TROP experiment are especially noteworthy for their implications regarding the use of the annular modes to determine the circulation responses to climate change (e.g., Gillett and Fyfe 2013). In an annular mode index, the jet position and jet strength are incorporated together into one measure of the annular mode. However, as Fig. 3c demonstrates, the seasonality of the jet position and strength responses to a tropical upper-tropospheric warming may not be the same. This difference is particularly strong in winter, the season most strongly associated with NAO/NAM patterns. Therefore, caution must be taken when linking seasonal trends in the annular modes to trends in the jet position and speed, as they do not necessarily vary in the same way in all seasons (e.g., Swart et al. 2015; Thomas et al. 2015).

b. *Assessing the linearity of the response*

In the real atmosphere, the projected thermal forcings due to climate change do not and will not occur in isolation. That is, the circulation will be forced by both tropical upper-tropospheric heating and polar lower-tropospheric heating at the same time. Therefore, while it is instructive to study the circulation's response to these two heatings separately (represented by the TROP and POLAR experiments), it is also worthwhile to study the linearity of the circulation response to the simultaneous application of TROP and POLAR. In this section, the response to these two concurrent forcings is compared to the superposition of the responses to the individual forcings in order to assess the linearity of the circulation response. The linearity of the circulation response to the strength of the heating is also briefly examined by adjusting the strength of the TROP and POLAR heating amplitudes (q_0).

A third experiment, BOTH, was run by applying both the TROP and POLAR heating experiments together (i.e., a simultaneous application of the heatings in Figs. 2a and 2b). If the circulation response to the BOTH experiment is similar to the addition of the TROP and POLAR responses, then the jet response to multiple heating sources would be considered linear; that is, the response can be accurately reconstructed by superimposing the separate responses of TROP and POLAR (referred to as TROP + POLAR). If, however, the responses of BOTH and TROP + POLAR are not similar, then the circulation response would be considered nonlinear with regard to the heating location. Such a comparison is made in Fig. 4. Figure 4a demonstrates that, while the jet position responses to BOTH and TROP + POLAR are comparable in December–January and in May–August, the response to BOTH is much greater (up to 3° latitude) in the transition seasons than the response to TROP + POLAR. The jet position response to multiple thermal forcings is thus quite nonlinear in the transition seasons. Additionally, note that in every month, the response to BOTH is equal to or larger than the response to TROP + POLAR. The poleward shift of the jet in response to TROP is larger, or, alternatively, the equatorward shift of the jet in response to POLAR is smaller, when the two forcings are applied in tandem than when they are applied individually.

The jet strength response, seen in Fig. 4b, also exhibits nonlinear behavior. As with the jet position response, the jet strength response is approximately linear in the winter and summer, and nonlinear in the transition seasons. This nonlinearity suggests a cancellation between the TROP and POLAR influence when the two occur simultaneously.

In addition to studying the nonlinearity of the jet response to heating in different locations, the circulation may also respond nonlinearly to the amplitude of the heating. To answer this question, an additional set of simulations is performed under March–October conditions. Both tropical upper-tropospheric heatings and polar lower-tropospheric heatings are applied individually, with the strength of the heating (q_0) varying from -1.0 to $+1.0\,\mathrm{K\,day^{-1}}$. Over the range of heating amplitudes tested, the response of the jet to the TROP experiment is nonlinear (not shown)—the jet position varies by over 15° for heating amplitudes between $\pm 0.2\,\mathrm{K\,day^{-1}}$, while heating amplitudes less than $-0.4\,\mathrm{K\,day^{-1}}$ and greater than $+0.8\,\mathrm{K\,day^{-1}}$ see little change in the position of the eddy driven jet. This behavior is consistent with previous studies—Fig. 13 in Barnes and Hartmann (2011) indicates that the relationship between the location of the ''baroclinic zone'' and the eddy-driven jet latitude in a barotropic model is not simply one-to-one; O'Rourke and Vallis (2013) also demonstrate a minimum zonal phase speed bound that restricts the eddy activity to certain regions; Butler et al. (2010) point out that in strong tropical heating cases, the maximum meridional temperature gradient may be shifted too far poleward, inhibiting the formation of the eddy-driven jet; and Barnes et al. (2010) suggest constraints on the jet latitude such as turning latitudes on the poleward flank [Barnes et al. (2010) and the references therein].

The jet position response to changes in the POLAR heating is not as large; over the range of values tested here, the jet response to variations in POLAR heating amplitude is approximately linear (not shown). The jet response to POLAR does not fully display the asymptotic behavior of the response to TROP, even in response to heating amplitudes as large as $\pm 3\,\mathrm{K\,day^{-1}}$ (not shown). This suggests that even for large values of q_0, the jet response to variations in the POLAR experiment does not exhibit the strongly nonlinear behavior in response to changes in heating magnitude exhibited by the response to the TROP experiment.

c. *Climatological jet position experiments*

The jet position response to an external forcing has been previously shown to be sensitive to the climatological position of the jet. For example, Kidston and Gerber (2010), Barnes et al. (2010), and Son et al. (2010) all find that models with a more equatorward Southern Hemisphere jet exhibit an enhanced response to an external forcing, such as increased CO_2 or loss of ozone. But does the sensitivity of the circulation to the basic state of the circulation, specifically the climatological position of the jet, matter more in some seasons than in others? In this set of experiments, the seasonal sensitivity of the circulation response to the climatological position of the jet is examined with the A+5, A+2, A−2, and A−5 experiments described in section 2d. In observations, the eddy-driven jets are not all located at the same latitudes—the North Atlantic jet is generally located farther poleward than the North Pacific jet, for example. GCMs are also known to exhibit large equatorward biases in the jet position (e.g., Kidston and Gerber 2010). Therefore, it is important to explore the seasonal sensitivity of the jet position response for jets with various climatological positions.

Figure 5a shows the jet position for the control runs for three mean state experiments (A+5, A+2, and A−2), and the model default configuration employed in the first set of experiments (referred to as DEFAULT). All four experiments in Fig. 5a exhibit similar seasonal cycles of the jet position, with the jet farthest poleward in the summer and more equatorward in winter. The experiments simply shift the mean jet position—A+5 and A+2 have jets poleward of the jet position DEFAULT, while the A−2 jet is equatorward of the DEFAULT jet. Both A+5 and A+2 have jets with a slightly suppressed seasonal cycle when compared with that of DEFAULT, while the A−2 jet exhibits an enhanced seasonal cycle. Experiment A−5 (not shown) has a jet that is far equatorward of DEFAULT in all months, with a jet that shifts as far south as 30°N in the transition seasons. Additionally, the A−5 jet position in December–January is approximately the same as the A−5 jet position in June–July. This behavior is not seen in DEFAULT, or in A+5, A+2, or A−2, all of which have jets that are significantly more poleward in summer than in winter. As the seasonal cycle of the jet position in A−5 deviates substantially from that of DEFAULT, A−5 will not be discussed further.

The jet position response to the TROP and POLAR experiments for A+ 5, A+2, and A−2 are compared to the responses of DEFAULT in Fig. 5b. All experiments in Fig. 5 exhibit a poleward shift of the jet in response to a tropical upper-tropospheric warming. Regardless of the climatological jet position, this poleward shift is largest in the transition seasons, and smallest in the winter and summer. The jet position experiment with the most equatorward jet, A−2 exhibits the largest response to the TROP experiment, shifting nearly 10°N in

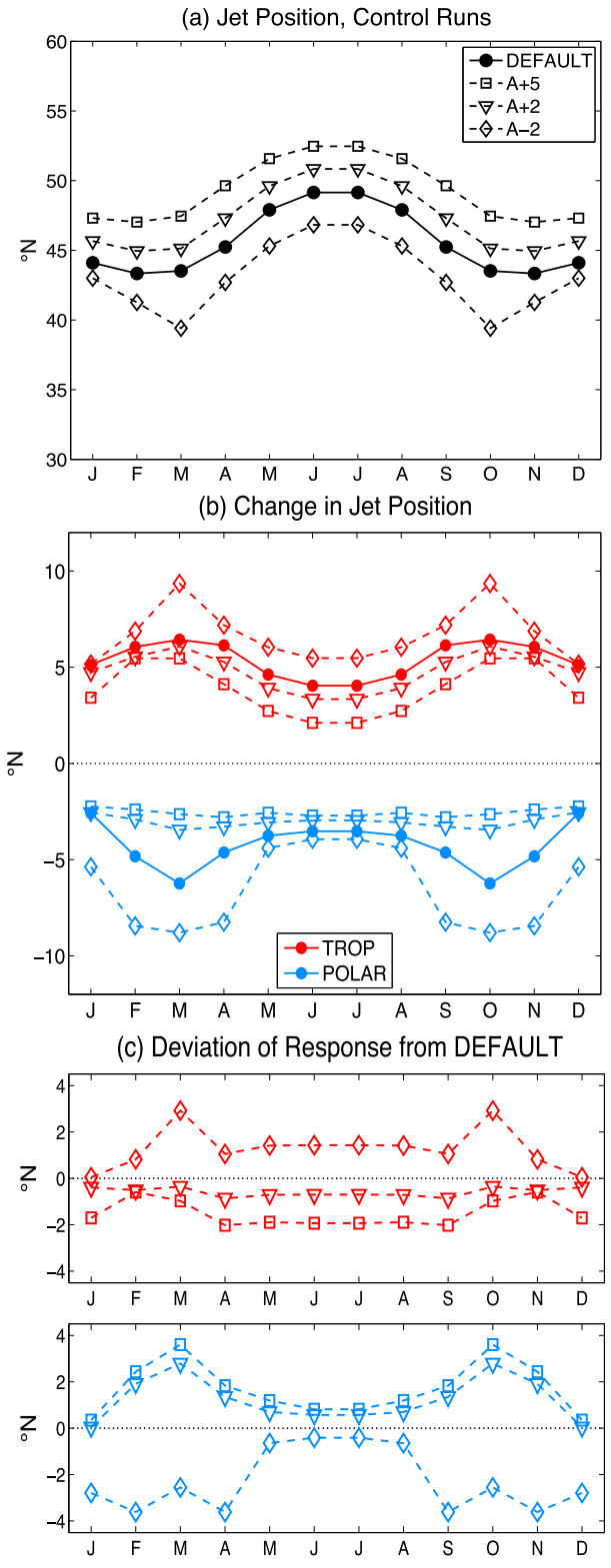

FIG. 5. (a) Jet position for control runs and (b) change in jet position for TROP and POLAR heating experiments for mean state experiments (A+5, A+2, and A−2) and model default (DEFAULT). (c) The difference in the jet position response for A+5, A+2, and A−2 compared to DEFAULT.

March–October. The experiment with the most poleward jet, A+5 exhibits the weakest response to the TROP experiment, with a maximum response of around 5°. So, while the magnitude of the jet response to tropical upper-tropospheric heating does exhibit some dependence on the climatological jet position, the overall seasonal sensitivity of the response appears to be similar, in that all four experiments peak in the transition seasons.

The four climatological jet position experiments all exhibit an equatorward shift of the jet in response to the polar lower-tropospheric warming (blue lines in Fig. 5b). The response of A−2, the most equatorward jet position, exhibits a similar seasonality to the DEFAULT response to the POLAR experiment, with the strongest response in the transition seasons. As was the case for the TROP heating, A−2 also exhibits the largest response. However, the two mean states that have jets poleward of the DEFAULT jet, A+2 and A+5, do not exhibit the same seasonality in their responses to POLAR. The A+2 and A+5 responses appear to have little seasonality, with all months shifting 1.5°–2° equatorward.

Is the jet response more sensitive to climatological jet latitude in some months versus others? To more clearly visualize these results, the deviation of the mean state experiment responses (A+5, A+2, and A−2) from the DEFAULT responses to the TROP and POLAR experiments were calculated. That is, the A+5, A+2, and A−2 responses are subtracted from the DEFAULT responses to TROP and to POLAR, and these deviations are shown in Fig. 5c. The deviations of the A+5 (red squares) and A+2 (red triangles) responses to the TROP heating experiment are approximately constant across all seasons, suggesting that the response is weakened by about the same amount every month compared to the DEFAULT response. The A−2 (red diamonds) response to the TROP experiment, however, does exhibit some seasonality. From April to September, the A−2 response is about 1.5° larger than the DEFAULT response to TROP. In March–October, however, the A−2 response is over 3° larger than the DEFAULT response to the same tropical heating. And from November to February, the A−2 response is nearly identical to the DEFAULT response to the TROP experiment. So, for the most equatorward jet, A−2, the jet response is more sensitive to the climatological jet position in March–October than in the other months of the year.

The deviations of all three mean state experiment responses—A+5 (blue squares), A+2 (blue triangles), and A−2 (blue diamonds)—to POLAR also exhibit a seasonality. All three experiments exhibit larger deviations from DEFAULT in the transition seasons

compared to the winter and summer. In fact, the deviation for all three mean state experiments is approximately zero in the summer months. This is not to say the circulation response to a polar lower-tropospheric warming is zero in the summer—Fig. 5b shows that the jet shifts equatorward in May–August around 2°. Rather, the mean state has little impact on the magnitude of this shift—no matter where the jet is climatologically located, it will shift equatorward about the same amount in response to a polar lower-tropospheric warming in the summer months. Additionally, no matter where the jet is climatologically located, its response will deviate more from that of DEFAULT in the transition seasons—a reduction in the equatorward shift of the jet for the A+5 and A+2 experiments (jets poleward of DEFAULT), and an increase in the equatorward shift of the jet for the A−2 experiment (a jet equatorward of DEFAULT).

4. Discussion

Why is there such a strong seasonal sensitivity in the circulation response to tropospheric warming in these idealized experiments? Although a full exploration of this question is beyond the scope of this work, one possible mechanism that could explain the jet position response is discussed here. Namely, the seasonality of the circulation response is a manifestation of a seasonality of the low-frequency variability of the circulation of the control climate. This idea stems from the application of fluctuation–dissipation theory to climate change studies (see Gerber et al. 2008; Shepherd 2014; Ring and Plumb 2007, 2008). In this context, fluctuation–dissipation theory suggests that the response of the atmosphere to an external perturbation is related to its internal variability. Specifically, larger internal variability will lead to a larger jet response that projects onto this variability. So, if the control simulations exhibit a greater jet variability in the transition seasons, one might expect these simulations to exhibit the largest response to thermal forcing in these seasons.

Following Gerber et al. (2008), the *e*-folding time (τ) of the autocorrelation function of the zonal mean zonal wind at 775 hPa is used to characterize the low-frequency variability. The zonal mean, latitude-weighted zonal wind at 775 hPa ($[U_{775}]$) was calculated using daily data (note that the previous sections used 30-day mean data). The τ is defined as the *e*-folding time of the first principal component time series of the leading EOF of $[U_{775}]$ (referred to as PC1). The τ is calculated by fitting a first-order polynomial to the autocorrelation function of PC1 around the approximate value of $1/e$. This analysis was applied to each month of the unforced experiments (i.e., the control runs for DEFAULT, A+5, A+2, and A−2). Because of computational constraints, the previous experiments only output monthly data; however, daily data were needed to calculate τ. Therefore, two new runs for each value of χ were run for each unforced experiment, outputting daily data. Twenty years of daily data were used to calculate each τ. Using Eq. (2.3) of Gerber et al. (2008), an integration length of 7200 days indicates that the standard deviation of τ is likely less than 1 day for nearly all months of all experiments. The *e*-folding times for each simulation were calculated separately, and then the simulations using the same value of χ were averaged together.

The values of τ_{PC1} for all four unforced experiments, seen in Fig. 6a, exhibit largely similar seasonal cycles to those of the jet position responses—the largest values of τ_{PC1} occur in the transition seasons. In most months (all months in the A+2 and A+5 experiments), the *e*-folding times are under 25 days [thought to be the intrinsic autocorrelation time scale for variations in the extratropical jet in the Held–Suarez system, as described by Gerber et al. (2008)]. However, in the DEFAULT and A−2 runs (the experiments with the most equatorward climatological jet positions), there are sharp increases in *e*-folding times in the transition months (February–November and March–October for A−2, and March–October for DEFAULT)—in these instances, τ jumps as high as 85 days. These unrealistically large *e*-folding times have been previously documented (e.g., Gerber et al. 2008), and are likely attributable to persistent extreme events. For example, in the months with unrealistically high values of $\tau(\tau > 30$ days), these persistent extreme events (events with a magnitude of PC1 that exceeds 2) can last as long as 100 days (not shown).

Next, the internal variability of the eddy-driven jet is decomposed further, by calculating the *e*-folding time of both the jet position and the jet strength independently. These separate *e*-folding times for jet position and jet strength can be seen in Figs. 6b and 6c, respectively. The jet position *e*-folding time (τ_{pos}, in Fig. 6b) is generally higher in the transition seasons, and lower in summer and winter. The seasonal cycle of the jet position *e*-folding time is similar to the seasonal cycle of the *e*-folding time of PC1 (Fig. 6a), and the seasonal cycle of the jet position response to heating (Fig. 3b). Additionally, the jet position *e*-folding time is generally higher for the jets with more equatorward mean states (DEFAULT and A−2), which is in agreement with previous studies suggesting that equatorward jets are more persistent (e.g., Barnes et al. 2010; Kidston and Gerber 2010). However, the high sensitivity of the *e*-folding time scales to extreme events remains—in March–October, the *e*-folding time of jet position jumps to about 50 days for DEFAULT, and about 65 days for A−2.

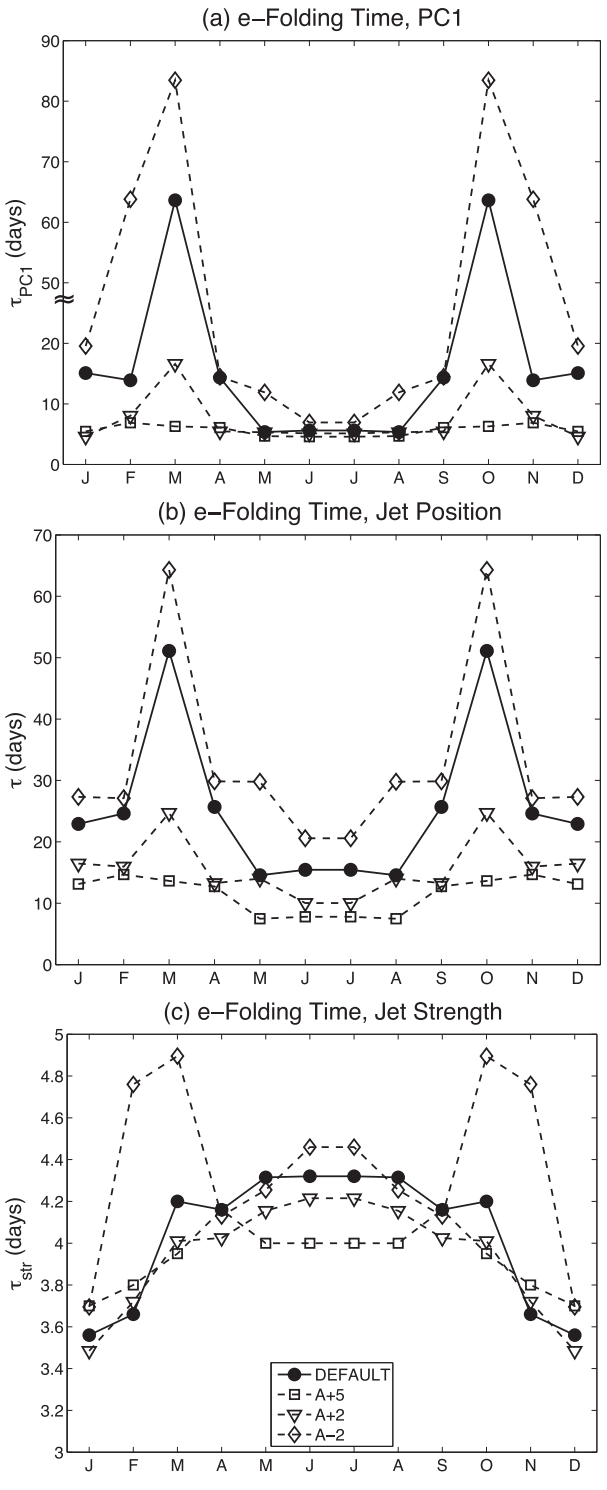

FIG. 6. The *e*-folding time (τ) for (a) PC1, (b) jet position, and (c) jet strength for model control runs. Note that the τ scale for (a) skips from 20 to 50 days.

The *e*-folding time of jet strength (τ_{str} in Fig. 6c) is generally higher in summer and lower in winter, following the seasonal cycle of the jet strength response to an upper-tropical tropospheric heating (red circles in Fig. 3c). Again, the *e*-folding time sharply increases in the transition seasons—this time, in February–November and March–October for A−2. Sharp increases in τ_{str} are also seen in March–October for DEFAULT, although the summertime values of τ_{str} are still larger for the DEFAULT experiment. So, while the τ_{pos} and τ_{PC1} exhibit similar seasonal sensitivities, τ_{str} does not. Additionally, the extremely high values of τ_{PC1} are likely driven by a combination of highly persistent variations of both jet latitude and jet speed. These results further suggest that jet position and jet strength should not be assumed to respond to forcing in the same way, as their variabilities do not exhibit the same seasonal cycles, at least in this idealized model.

As the *e*-folding calculation is clearly sensitive to extreme events, it is beneficial to quantify the internal variability of the circulation using another metric that is less sensitive to these extremes. The spread metric is defined as the difference between the 90th percentile and 10th percentile of a quantity—in this case, jet position and jet strength. Simply put, the jet position spread estimates the size of the range of latitudes over which the jet can be found on 80% of days, while the jet strength spread gives the range of strengths of the jet on 80% of days.

The jet position spread and jet strength spread can be seen in Figs. 7a and 7b, respectively. The jet position spread (Fig. 7a) shares the same seasonal cycle as the jet position *e*-folding time (Fig. 6b) and the jet position response to heating (Fig. 3b). The jet position spread is greatest in the transition seasons, and lowest in the summer. Although the jet position spread is greatest in the transition seasons, it does not sharply increase to extreme values the way jet position *e*-folding time did. The jet strength spread, does not exhibit the same seasonal cycle as the jet strength response to heating (Fig. 3c), or the jet strength *e*-folding time (Fig. 6c). The jet strength spread is greatest in winter and lowest in summer in all experiments, and is also greatest for the more poleward climatological jet positions (A+2 and A+5). The A+2 and A+5 jets are stronger in every month than the DEFAULT and A−2 jets (not shown), so Fig. 7b suggests that weaker jets (more equatorward jets, summertime jets) have lower variability than stronger jets (more poleward jets, wintertime jets).

Both the *e*-folding time scales and the jet position spreads suggest that the jet position response to anthropogenic forcing is greatest in months with the greatest internal variability—in this case, the transition

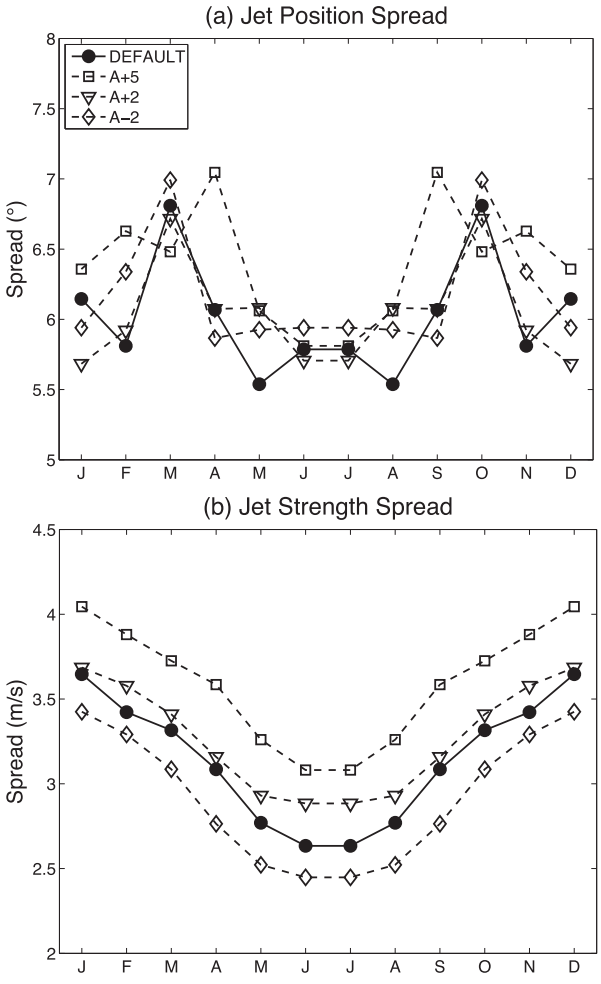

FIG. 7. Spread for (a) jet position and (b) jet strength for model control runs.

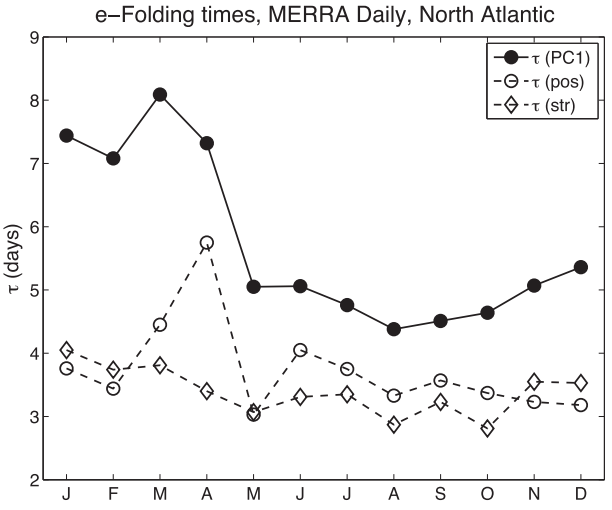

FIG. 8. Jet position, jet strength, and PC1 *e*-folding times for daily MERRA reanalysis data.

seasons. The implications for the jet strength response are less clear. The jet strength *e*-folding time scales are generally greatest in the summer, matching the seasonal cycle of the jet strength response to tropical upper-tropospheric warming (the TROP experiment). However, some experiments (A−2, and DEFAULT to a lesser extent) do exhibit sharp increases in jet strength *e*-folding times in the transition seasons, more closely mirroring the seasonal cycle of the jet strength response to polar lower-tropospheric warming (the POLAR experiment). These results suggest that the jet position response is well correlated with the internal variability of the jet, while the jet strength response is less so.

Finally, the *e*-folding time of the first principal component time series of the lower-level winds (PC1), and jet position and strength *e*-folding times are calculated for MERRA reanalysis data over the North Atlantic (defined as 15°–75°N, 0°–70°W) for comparison with the idealized model. Although the observed Southern Hemisphere jet is more zonally symmetric than the North Atlantic jet, its recent trends have been strongly influenced by trends in stratospheric ozone, which has a seasonality of its own (e.g., Thompson and Solomon 2002); therefore, the North Atlantic is used for this example. The three persistence metrics were computed for daily MERRA reanalysis data using the procedures described in section 2e, although a 3-month moving average was used to calculate each month's *e*-folding time in the MERRA reanalysis data (i.e., the January *e*-folding time was calculated from daily data in DJF, the February *e*-folding time was calculated from daily JFM data, and so on). This analysis is not intended to quantify the extent to which the zonally symmetric idealized model results can emulate the observed variability of the North Atlantic jet. Rather, the aim of this analysis is to demonstrate that the internal variability of the observed eddy-driven jet also exhibits significant seasonality, and to show that the broad conclusions from these idealized modeling experiments may in fact have relevance to the future responses of the jets.

Figure 8 displays the MERRA North Atlantic PC1 *e*-folding time (filled black circles), jet position *e*-folding time (open black circles), and jet strength *e*-folding time (open black diamonds). Figure 8 indicates that, as in the dry core results, the jet position and PC1 *e*-folding times for the North Atlantic reanalysis data display similar seasonal cycles, with both peaking in late winter/early spring and decreasing in the summer. The contrast between winter and summer *e*-folding time scales is greater in τ_{PC1} than it is in τ_{pos}, with τ_{PC1} reaching 7–8 days in January through April and remaining around 5 days the rest of the year, while τ_{pos} only exceeds 4 days in March and April. The seasonal cycle of the jet strength *e*-folding time is flatter than those of τ_{PC1} and τ_{pos},

although τ_{str} is slightly higher in the winter and lower in the summer. Figure 8 indicates that the internal variability of the observed North Atlantic jet does in fact have a seasonal cycle, and thus, the idealized model results may be used to provide insights regarding the observed jet streams.

The mechanisms that explain the seasonal sensitivity of the jet response to the idealized heating experiments are complex, and far from fully explored here. However, taken together, the seasonalities of the persistence of the jet's internal variability (*e*-folding time) and the jet position spread provide some insight into the circulation's seasonal sensitivity described in this paper. Generally speaking, the *e*-folding times and jet position spreads are greater in the spring and fall—the months that exhibit the largest jet position responses to tropospheric warming. This suggests that the internal variability of the unforced circulation may play at least some part in determining the seasonality of the jet position response—months with greater internal variability are more likely to exhibit a larger jet position response to an external heating. Regarding the jet strength response, as the seasonal sensitivities of the responses to the TROP and POLAR experiments are different, the response cannot be described by fluctuation–dissipation theory alone. Rather, while the seasonal cycle of internal variability may be able to explain the response to TROP, the jet speed response to POLAR does not resemble the response that would be predicted by fluctuation–dissipation.

5. Conclusions

This study addresses the following questions: ''What is the seasonal sensitivity of the circulation to tropospheric heating anomalies?'' and ''How does the climatological jet position impact the circulation's seasonal sensitivity?'' The GFDL dry dynamical core is used to address these questions in an idealized framework. A seasonal cycle was applied in the model by adjusting the relaxation temperature profile to capture each month of the year. Two heating anomalies, a tropical upper-tropospheric heating (TROP) and a polar lower-tropospheric heating (POLAR), were applied to a variety of climatological jet positions—the model default and three adjusted jet positions (A+5, A+2, and A−2). The linearity of the circulation response to these thermal forcings was also assessed by applying both the TROP and POLAR experiments to the model default configuration simultaneously, and by adjusting the strengths of the individual TROP and POLAR experiments. With this suite of experiments, the seasonality of the circulation response to two identical heating profiles and the impact of the mean state of the circulation on these responses were explored. These experiments demonstrate the following:

1) There is a seasonal sensitivity in the jet position response to identical forcing, with the transition seasons exhibiting the largest circulation response for both the TROP and POLAR experiments.
2) When forced with two heatings at once (TROP and POLAR), the circulation response is nonlinear in the transition seasons, and approximately linear in the winter and the summer.
3) The seasonal sensitivity of the circulation response to the TROP experiment is greatest in the transition seasons regardless of the climatological jet position. The seasonal sensitivity of the circulation response to the POLAR experiment, however, does exhibit dependence on the climatological jet position, with more poleward jets displaying less seasonal sensitivity than more equatorward jets in response to the POLAR experiment.
4) The months with the greatest jet position response are also the months with the greatest internal variability, suggesting that fluctuation–dissipation theory may explain, at least in part, the jet position response to forcing. The relationship between the internal variability and the jet strength response is less clear.

Although these results were obtained in the very idealized environment of a dry dynamical core, they likely extend to more realistic models, and even to observations. This study has shown that relatively minor changes to the circulation, such as those brought on by a seasonal cycle, can have large impacts on the circulation response even when only dry dynamics are considered. Even though the real world circulation exhibits seasonality driven by additional factors (e.g., land–sea contrast, stratospheric variability) not represented here, when evaluated in the context of climate variability and climate change, these results suggest the following:

1) The sign of the jet position response to a tropical upper-tropospheric heating (TROP) and a polar lower-tropospheric heating (POLAR) is robust across all 12 months of the year, shifting poleward in response to a tropical upper-level heating and equatorward in response to a polar lower-level heating. However, the magnitude of this response varies with season. Thus, studies looking only at one particular season, or the annual mean, may underestimate or overestimate the responses in other seasons.
2) The importance of the climatological jet position on the amplitude of the response highlights the importance of correctly modeling the mean state of the jet in the GCMs in order to fully estimate the magnitude and

seasonality of the circulation response. Previous studies have noted an equatorward bias in jet latitude in climate models (e.g., Kidston and Gerber 2010; Barnes and Polvani 2013), with more equatorward jets shifting more than their poleward counterparts. The results presented here are in agreement with these studies. However, these results highlight that the importance of this bias is not necessarily the same across seasons.

3) The circulation response to the simultaneously applied TROP and POLAR experiments is not linear in all seasons. Therefore, model simulations with only one forcing may obtain very different results than what might occur under climate change, although this depends on the season. In some seasons, the circulation response may be approximately linear, and the full circulation response can be assumed to be a simple superposition of the responses to the individual heatings.

The circulation response to seasonally invariant tropospheric warming has a robust seasonality. However, projected tropospheric warming (e.g., Arctic amplification) also has a seasonality of its own. Thus, a thorough understanding of both of these components of the seasonality—forcing and the circulation sensitivity—separately, will ultimately lead toward an understanding of the full circulation response and the dynamics that drive it.

Acknowledgments. This work was funded, in part, by a grant from the National Science Foundation's Climate and Large-Scale Dynamics Program. The MERRA reanalysis data used in this study have been publicly provided by the Global Modeling and Assimilation Office (GMAO) at NASA Goddard Space Flight Center through the NASA GES DISC online archive (http://disc.sci.gsfc.nasa.gov/daac-bin/DataHoldings.pl). The authors would also like to thank three anonymous reviewers for their assistance in improving this work.

APPENDIX

Tropospheric Seasonal Cycle in the GFDL Dynamical Core

Recall the equation for the tropospheric equilibrium temperature profile is

$$T_{\mathrm{eq}}^{\mathrm{trop}}(p,\phi) = \max\left[200\,K, \left\{T_0 - \left[(\Delta T)_y \sin\phi^2 + \varepsilon \sin\phi + (\Delta T)_z \log\left(\frac{p}{p_0}\right)\cos\phi^2\right]\right\}\left(\frac{p}{p_0}\right)^{\kappa}\right], \tag{A1}$$

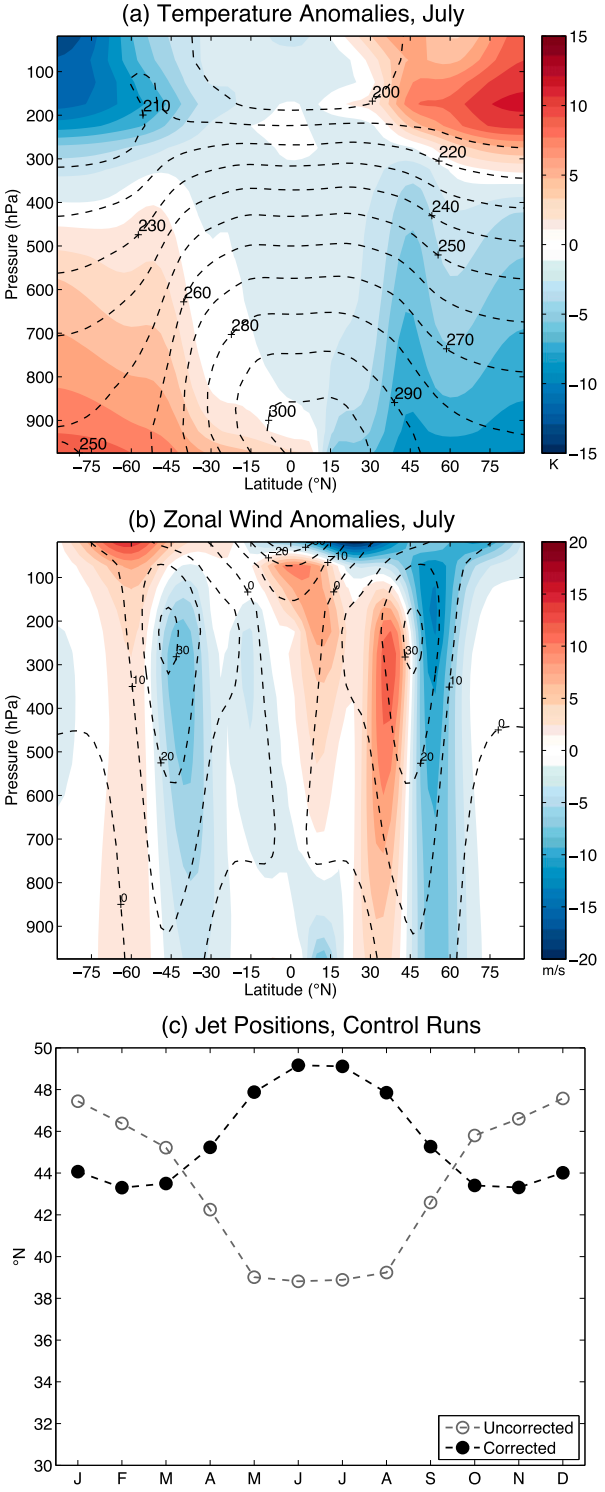

FIG. A1. Comparison of corrected and uncorrected model for (a) July temperature, (b) July zonal wind, and (c) monthly mean jet position. The dashed lines in (a) and (b) are the corrected temperature and zonal wind contours, and the colors are the anomalies (uncorrected − corrected).

which specifies that T_{eq}^{trop} cannot be lower than 200 K. However, in the posted current version of the GFDL dry dynamical core., this lower bound on the temperature (here called T_{min}) is allowed to vary with season:

$$T_{min} = 200 - \varepsilon \sin\phi. \quad \text{(A2)}$$

For example, for $\varepsilon = 20$ K and $\phi = 90°$ (winter solstice at the North Pole), T_{min} would be 180 K. This seasonal variation allows the upper levels in the winter hemisphere to cool below 200 K, which shifts the jet slightly poleward. However, the greater impact of this variation occurs in the summer hemisphere, which is allowed to warm excessively, as seen in Figure A1a, which compares the uncorrected [T_{min} varies with season, as in (A2)] and corrected [T_{min} cannot drop below 200 K, as in (A1)] model temperature profiles. This excessive stratospheric warming shifts the summer hemisphere jet much too far equatorward—in some months, as much as 10°, as seen in Fig. A1b. This large equatorward bias in the summer jet position also results in an opposite seasonal cycle of the jet. In Fig. A1c, the uncorrected jet (open circles) is most poleward in winter and most equatorward in summer, which is in opposition to observations (e.g., Hannachi et al. 2013). The corrected jet (closed circles), on the other hand, exhibits a jet seasonal cycle that is comparable to the observed jet seasonal cycle. This issue only affects the troposphere-only model configuration—when the model is run with a stratosphere, the temperature is not constrained by the maximum function in (A1), as the presence of stratospheric dynamics allows the model to set its own temperature [see Polvani and Kushner (2002) and Kushner and Polvani (2006) for more details about the stratospheric dynamics].

REFERENCES

Barnes, E. A., and D. L. Hartmann, 2011: Rossby wave scales, propagation, and the variability of eddy-driven jets. *J. Atmos. Sci.*, **68**, 2893–2908, doi:10.1175/JAS-D-11-039.1.

——, and L. M. Polvani, 2013: Response of the midlatitude jets and of their variability to increased greenhouse gases in the CMIP5 models. *J. Climate*, **26**, 7117–7135, doi:10.1175/JCLI-D-12-00536.1.

——, and D. W. J. Thompson, 2014: Comparing the roles of barotropic versus baroclinic feedbacks in the atmosphere's response to mechanical forcing. *J. Atmos. Sci.*, **71**, 177–194, doi:10.1175/JAS-D-13-070.1.

——, D. L. Hartmann, D. M. W. Frierson, and J. Kidston, 2010: Effect of latitude on the persistence of eddy-driven jets. *Geophys. Res. Lett.*, **37**, L11804, doi:10.1029/2010GL043199.

Butler, A. H., D. W. J. Thompson, and R. Heikes, 2010: The steady-state atmospheric circulation response to climate change–like thermal forcings in a simple general circulation model. *J. Climate*, **23**, 3474–3496, doi:10.1175/2010JCLI3228.1.

——, ——, and T. Birner, 2011: Isentropic slopes, downgradient eddy fluxes, and the extratropical atmospheric circulation response to tropical tropospheric heating. *J. Atmos. Sci.*, **68**, 2292–2305, doi:10.1175/JAS-D-10-05025.1.

Chen, G., and I. M. Held, 2007: Phase speed spectra and the recent poleward shift of Southern Hemisphere surface westerlies. *Geophys. Res. Lett.*, **34**, L21805, doi:10.1029/2007GL031200.

——, and R. A. Plumb, 2014: Effective isentropic diffusivity of tropospheric transport. *J. Atmos. Sci.*, **71**, 3499–3520, doi:10.1175/JAS-D-13-0333.1.

Cohen, J., M. Barlow, P. Kushner, and K. Saito, 2007: Stratosphere–troposphere coupling and links with Eurasian land surface variability. *J. Climate*, **20**, 5335–5343, doi:10.1175/2007JCLI1725.1.

Collins, M., and Coauthors, 2013: Long-term climate change: Projections, commitments and irreversibility. *Climate Change 2013: The Physical Science Basis*, T. F. Stocker et al., Eds., Cambridge University Press, 1029–1136, doi:10.1017/CBO9781107415324.024.

Davis, N. A., and T. Birner, 2013: Seasonal to multidecadal variability of the width of the tropical belt. *J. Geophys. Res. Atmos.*, **118**, 7773–7787, doi:10.1002/jgrd.50610.

Deser, C., R. A. Tomas, M. Alexander, and D. Lawrence, 2010: The seasonal atmospheric response to projected Arctic sea ice loss in the late twenty-first century. *J. Climate*, **23**, 333–351, doi:10.1175/2009JCLI3053.1.

——, ——, and L. Sun, 2015: The role of ocean–atmosphere coupling in the zonal-mean atmospheric response to Arctic sea ice loss. *J. Climate*, **28**, 2168–2186, doi:10.1175/JCLI-D-14-00325.1.

Eichelberger, S. J., and D. L. Hartmann, 2007: Zonal jet structure and the leading mode of variability. *J. Climate*, **20**, 5149–5163, doi:10.1175/JCLI4279.1.

Garfinkel, C. I., D. W. Waugh, and E. P. Gerber, 2013: The effect of tropospheric jet latitude on coupling between the stratospheric polar vortex and the troposphere. *J. Climate*, **26**, 2077–2095, doi:10.1175/JCLI-D-12-00301.1.

Gerber, E. P., S. Voronin, and L. M. Polvani, 2008: Testing the annular mode autocorrelation time scale in simple atmospheric general circulation models. *Mon. Wea. Rev.*, **136**, 1523–1536, doi:10.1175/2007MWR2211.1.

Gillett, N. P., and J. C. Fyfe, 2013: Annular mode changes in the CMIP5 simulations. *Geophys. Res. Lett.*, **40**, 1189–1193, doi:10.1002/grl.50249.

Hannachi, A., E. A. Barnes, and T. Woollings, 2013: Behaviour of the winter North Atlantic eddy-driven jet stream in the CMIP3 integrations. *Climate Dyn.*, **41**, 995–1007, doi:10.1007/s00382-012-1560-4.

Harvey, B. J., L. C. Shaffrey, and T. J. Woollings, 2014: Equator-to-pole temperature differences and the extra-tropical storm track responses of the CMIP5 climate models. *Climate Dyn.*, **43**, 1171–1182, doi:10.1007/s00382-013-1883-9.

Held, I. M., 1993: Large-scale dynamics and global warming. *Bull. Amer. Meteor. Soc.*, **74**, 228–241, doi:10.1175/1520-0477(1993)074<0228:LSDAGW>2.0.CO;2.

——, and M. J. Suarez, 1994: A proposal for the intercomparison of the dynamical cores of atmospheric general circulation models. *Bull. Amer. Meteor. Soc.*, **75**, 1825–1830, doi:10.1175/1520-0477(1994)075<1825:APFTIO>2.0.CO;2.

Holland, M. M., and C. M. Bitz, 2003: Polar amplification of climate change in coupled models. *Climate Dyn.*, **21**, 221–232, doi:10.1007/s00382-003-0332-6.

Kidston, J., and E. P. Gerber, 2010: Intermodel variability of the poleward shift of the austral jet stream in the CMIP3 in-

tegrations linked to biases in 20th century climatology. *Geophys. Res. Lett.*, **37**, L09708, doi:10.1029/2010GL042873.

Kushner, P. J., and L. M. Polvani, 2004: Stratosphere–troposphere coupling in a relatively simple AGCM: The role of eddies. *J. Climate*, **17**, 629–639, doi:10.1175/1520-0442(2004)017<0629:SCIARS>2.0.CO;2.

——, and ——, 2006: Stratosphere–troposphere coupling in a relatively simple AGCM: Impact of the seasonal cycle. *J. Climate*, **19**, 5721–5727, doi:10.1175/JCLI4007.1.

O'Rourke, A. K., and G. K. Vallis, 2013: Jet interaction and the influence of a minimum phase speed bound on the propagation of eddies. *J. Atmos. Sci.*, **70**, 2614–2628, doi:10.1175/JAS-D-12-0303.1.

Polvani, L. M., and P. J. Kushner, 2002: Tropospheric response to stratospheric perturbations in a relatively simple general circulation model. *Geophys. Res. Lett.*, **29**, 1114, doi:10.1029/2001GL014284.

Rienecker, M. M., and Coauthors, 2011: MERRA: NASA's Modern-Era Retrospective Analysis for Research and Applications. *J. Climate*, **24**, 3624–3648, doi:10.1175/JCLI-D-11-00015.1.

Ring, M. J., and R. A. Plumb, 2007: Forced annular mode patterns in a simple atmospheric general circulation model. *J. Atmos. Sci.*, **64**, 3611–3626, doi:10.1175/JAS4031.1.

——, and ——, 2008: The response of a simplified GCM to axisymmetric forcings: Applicability of the fluctuation–dissipation theorem. *J. Atmos. Sci.*, **65**, 3880–3898, doi:10.1175/2008JAS2773.1.

Screen, J. A., and I. Simmonds, 2010: The central role of diminishing sea ice in recent Arctic temperature amplification. *Nature*, **464**, 1334–1337, doi:10.1038/nature09051.

Shaw, T., and A. Voigt, 2015: Tug of war on summertime circulation between radiative forcing and sea surface warming. *Nat. Geosci.*, **8**, 560–566, doi:10.1038/ngeo2449.

Shepherd, T. G., 2014: Atmospheric circulation as a source of uncertainty in climate change projections. *Nat. Geosci.*, **7**, 703–708, doi:10.1038/ngeo2253.

Sheshadri, A., R. A. Plumb, and E. P. Gerber, 2015: Seasonal variability of the polar stratospheric vortex in an idealized AGCM with varying tropospheric wave forcing. *J. Atmos. Sci.*, **72**, 2248–2266, doi:10.1175/JAS-D-14-0191.1.

Simpson, I. R., M. Blackburn, J. D. Haigh, and S. Sparrow, 2010: The impact of the state of the troposphere on the response to stratospheric heating in a simplified GCM. *J. Climate*, **23**, 6166–6185, doi:10.1175/2010JCLI3792.1.

——, ——, and ——, 2012: A mechanism for the effect of tropospheric jet structure on the annular mode–like response to stratospheric forcing. *J. Atmos. Sci.*, **69**, 2152–2170, doi:10.1175/JAS-D-11-0188.1.

——, T. G. Shepherd, P. Hitchcock, and J. F. Scinocca, 2013: Southern annular mode dynamics in observations and models. Part II: Eddy feedbacks. *J. Climate*, **26**, 5220–5241, doi:10.1175/JCLI-D-12-00495.1.

Son, S.-W., and S. Lee, 2005: The response of the westerly jets to thermal driving in a primitive equation model. *J. Atmos. Sci.*, **62**, 3741–3757, doi:10.1175/JAS3571.1.

——, and Coauthors, 2010: Impact of stratospheric ozone on Southern Hemisphere circulation change: A multimodel assessment. *J. Geophys. Res.*, **115**, D00M07, doi:10.1029/2010JD014271.

Swart, N. C., J. C. Fyfe, N. Gillett, and G. J. Marshall, 2015: Comparing trends in the southern annular mode and surface westerly jet. *J. Climate*, **28**, 8840–8859, doi:10.1175/JCLI-D-15-0334.1.

Tandon, N. F., L. M. Polvani, and S. M. Davis, 2011: The response of the tropospheric circulation to water vapor–like forcings. *J. Climate*, **24**, 5713–5720, doi:10.1175/JCLI-D-11-00069.1.

Thomas, J. L., D. W. Waugh, and A. Gnanadesikan, 2015: Southern Hemisphere extratropical circulation: Recent trends and natural variability. *Geophys. Res. Lett.*, **42**, 5508–5515, doi:10.1002/2015GL064521.

Thompson, D. W. J., and S. Solomon, 2002: Interpretation of recent Southern Hemisphere climate change. *Science*, **296**, 895–899, doi:10.1126/science.1069270.

——, and T. Birner, 2012: On the linkages between the tropospheric isentropic slope and eddy fluxes of heat during Northern Hemisphere winter. *J. Atmos. Sci.*, **69**, 1811–1823, doi:10.1175/JAS-D-11-0187.1.

Wang, S., E. P. Gerber, and L. M. Polvani, 2012: Abrupt circulation responses to tropical upper-tropospheric warming in a relatively simple stratosphere-resolving AGCM. *J. Climate*, **25**, 4097–4115, doi:10.1175/JCLI-D-11-00166.1.

Woollings, T., A. Hannachi, and B. Hoskins, 2010: Variability of the North Atlantic eddy-driven jet stream. *Quart. J. Roy. Meteor. Soc.*, **136**, 856–868, doi:10.1002/qj.625.

Wu, Y., and K. L. Smith, 2016: Response of Northern Hemisphere midlatitude circulation to Arctic amplification in a simple atmospheric general circulation model. *J. Climate*, **29**, 2041–2058, doi:10.1175/JCLI-D-15-0602.1.

Yin, J. H., 2005: A consistent poleward shift of the storm tracks in simulations of 21st century climate. *Geophys. Res. Lett.*, **32**, L18701, doi:10.1029/2005GL023684.